A scale-dependent cascade model for the 1/f spectrum in the pristine solar wind

M. Brodiano[1,2], F. Sahraoui[3], D. Manzini[4], L. Z. Hadid[3], F. Pugliese[1,2], P. Dmitruk[1,2,5], and N. Andrés[1,2,5]

[1] Universidad de Buenos Aires, Facultad de Ciencias Exactas y Naturales, Departamento de Física, Ciudad Universitaria, 1428 Buenos Aires, Argentina
[2] CONICET - Universidad de Buenos Aires, Instituto de Física Interdisciplinaria y Aplicada (INFINA), Ciudad Universitaria, 1428 Buenos Aires, Argentina
[3] Laboratoire de Physique des Plasmas (LPP), CNRS, École Polytechnique, Sorbonne Université, Université Paris-Saclay, Observatoire de Paris, 91120 Palaiseau, France
[4] Department of Physics and Astronomy, Queen Mary University of London, London E1 4NS, UK
[5] Institut Franco-Argentin de Dynamique des Fluides pour l'Environnement (IFADyFE), Universidad de Buenos Aires, CONICET, CNRS (IRL 2027), Buenos Aires, Argentina

July 10, 2026

ABSTRACT

Context. The solar wind provides a natural laboratory for studying turbulent plasmas over a broad range of temporal and spatial scales. Its low-frequency magnetic spectrum often displays a $1/f$ range, whose physical origin and connection to nonlinear turbulent transfer remain open questions.
Aims. We investigate whether the $1/f$ range can be interpreted as a turbulent range with scale-dependent energy transfer, and how this behavior differs from the inertial range. A central point of this work is that third-order structure functions can provide a useful estimate of the nonlinear energy transfer even when the inferred transfer rate is not scale independent.
Methods. We used in situ Parker Solar Probe measurements to compute the energy transfer rate from the incompressible magnetohydrodynamics third-order law, including expansion terms, and analyzed magnetic field increment statistics through probability density functions and structure functions. In particular, we used the third-order law as a diagnostic tool to investigate whether nonlinear energy transfers are present and how they scale with ℓ, rather than assuming a priori that the $1/f$ range behaves as a classical inertial range with constant flux.
Results. The energy transfer decreases approximately as $1/\tau$ (where τ is the time lag) within the $1/f$ range, in contrast with the nearly constant cascade rate expected in the inertial range. A scale-dependent model predicts an energy transfer across scales $\varepsilon_\ell \sim 1/\ell$, consistent with a k^{-1} magnetic spectrum. The statistics of magnetic field increments show intermittent signatures, especially in the parallel component, whereas the perpendicular fluctuations are found to be quasi-Gaussian.
Conclusions. These results suggest that the $1/f$ range can be interpreted as a non-conservative scale-dependent turbulent cascade, with implications for the interpretation of large-scale fluctuations in the solar wind and planetary magnetosheaths.

Key words. solar wind - magnetohydrodynamics (MHD) - turbulence - plasmas - methods: data analysis

1. Introduction

The solar wind is a unique laboratory for studying an astrophysical plasma that is in a fully developed turbulent state because a wide range of temporal and spatial scales are involved (Bruno & Carbone 2013; Verscharen et al. 2018; Sahraoui et al. 2020). One of the key methods for characterizing the multiscale nature of turbulence is through the power spectral density (PSD) of the turbulent fluctuations. In the solar wind, the low-frequency part of the PSD typically follows a -1 power-law exponent; in contrast, it steepens to $\sim -5/3$ (e.g., Case et al. 2020) within the inertial range. The origin of the $1/f$ range (also known as the energy-containing scales or the $1/f$ flicker noise) remains an open question (Matthaeus & Goldstein 1986; Velli et al. 1989; Dmitruk & Matthaeus 2007; Bemporad et al. 2008; Verdini et al. 2012; Matteini et al. 2018; Chandran 2018; Magyar & Doorsselaere 2022; Huang et al. 2023; Chen et al. 2020). Several efforts have been made to explain the emergence of the $1/f$ spectrum. Examples are the superposition of signals from uncorrelated magnetic reconnection events that occur in the corona, with their correlation times following a log-normal distribution (Matthaeus & Goldstein 1986); the evolution of Alfvén waves originating from the corona in the expanding solar wind (Velli et al. 1989; Verdini et al. 2012; Perez & Chandran 2013); the nonlinear evolution of the parametric instability, which leads to an inverse cascade of the Alfvén wave quanta (Chandran 2018); and the cutoff in the distribution of the fluctuations and the saturation of their mean amplitude in Alfvénic fast streams (Matteini et al. 2018).

We take a different approach here and attempt to determine whether the $1/f$ range is populated by fully developed turbulent fluctuations, and if this is so, why it does not exhibit a $-5/3$ scaling as the inertial range does, in agreement with predictions of magnetohydrodynamic (MHD) turbulence theory. To this end, we fully characterize the $1/f$ range as measured by Parker Solar Probe (PSP) (Fox et al. 2016) in the inner heliosphere, using the third-order law model of incompressible MHD turbulence (Politano & Pouquet 1998b,a; Sorriso-Valvo et al. 2002; Mininni & Pouquet 2009; Boldyrev et al. 2009; Wan et al. 2010; Verdini & Grappin 2015; Sorriso-Valvo et al. 2007;

Article published by EDP Sciences, to be cited as https://doi.org/10.1051/0004-6361/202660718

Sahraoui 2008; Coburn et al. 2015; Simakov & Chacón 2008; Masters et al. 2008; Matthaeus et al. 1999; MacBride et al. 2008; MacBride et al. 2005; Hadid et al. 2017, 2015; Andrés et al. 2018; Brodiano et al. 2023; Andrés et al. 2022), quantifying the level of intermittency therein and comparing the results with those from the inertial range.

2. Third-order law of incompressible MHD turbulence

From the MHD equations (e.g., Biskamp 2003) and following the usual assumptions of time stationarity and space homogeneity, scale separation between forcing and dissipation, and infinite kinetic and magnetic Reynolds numbers (e.g., Andrés & Sahraoui 2017), an exact relation for incompressible MHD turbulence can be derived (Politano & Pouquet 1998b,a),

$$-4\,\varepsilon \;=\; \rho_0\,\boldsymbol{\nabla}\cdot\langle[(\delta\mathbf{u})^2+(\delta\mathbf{b})^2]\,\delta\mathbf{u}\;-\;2\,(\delta\mathbf{u}\cdot\delta\mathbf{b})\,\delta\mathbf{b}\rangle, \tag{1}$$

where ε is the mean nonlinear energy transfer rate per unit volume, ρ_0 is the mean mass density, $\mathbf{u}$ is the velocity field, and $\mathbf{b}$ is the magnetic field in Alfvénic units. The operator δ denotes the field increment between two positions, $\mathbf{x}$ and $\mathbf{x}' = \mathbf{x} + \boldsymbol{\ell}$, with $\ell = |\boldsymbol{\ell}|$ the longitudinal distance. The angular bracket $\langle\cdot\rangle$ denotes an ensemble average, here replaced by a time average under the assumption of ergodicity (e.g., Biskamp 2003). It is important to mention that Eq. (1) is rooted in the von Kármán-Howarth energy balance and therefore should not be interpreted as requiring a scale-independent transfer rate from the outset. A constant value of ε is the particular outcome expected in a classical inertial range, where the energy flux is conservative across scales and the contributions from large-scale forcing, explicit time dependence, and dissipation are negligible within the range considered. If the third-order structure function instead yields a systematic dependence on ℓ, this does not by itself imply a conservative turbulent cascade. Rather, it indicates that the scale-by-scale energy balance is not in the standard inertial-range limit, and that the third-order contribution should be interpreted as an effective scale-dependent transfer estimate, possibly coexisting with time-dependent, forcing, expansion, or other large-scale contributions. A more general discussion of the relation between $\varepsilon(\ell)$ and cross-scale energy transfer is given in (Manzini et al. 2022). When we further assume statistical isotropy, we can integrate Eq. (1) over a sphere of radius ℓ to obtain a scalar relation valid for isotropic turbulence,

$$-\frac{4}{3}\,\varepsilon\,\ell \;=\; \rho_0\,\langle[(\delta\mathbf{u})^2+(\delta\mathbf{b})^2]\,\delta u_\ell\;-\;2\,(\delta\mathbf{u}\cdot\delta\mathbf{b})\,\delta b_\ell\rangle. \tag{2}$$

Solar wind turbulence is known to be anisotropic with respect to the local magnetic field. Therefore, strict isotropy is not expected to hold in observational data. However, for single-spacecraft measurements, the isotropic form of the third-order law is commonly employed to estimate the transfer rate along the sampling direction. This approach relies on the assumption that the dominant contribution to the divergence term can still be captured by the longitudinal increments projected along the flow direction. It has been extensively used in previous observational studies of solar wind turbulence (Sorriso-Valvo et al. 2007; Marino et al. 2008; Stawarz et al. 2009; Hadid et al. 2017; Bandyopadhyay et al. 2020; Andrés et al. 2018, 2022; Brodiano et al. 2023; Romanelli et al. 2024), and has been shown to provide meaningful estimates of the scale-to-scale energy transfer despite the presence of anisotropy.

When Eq. (2) is applied to single-spacecraft data, the Taylor hypothesis is used to convert time lags into spatial lags, that is, $\ell = \tau U_0$, where τ is the temporal lag, and U_0 is the mean plasma flow velocity. The longitudinal components of the fields are then defined as $u_\ell = \mathbf{u}\cdot\hat{\mathbf{U}}_0$ and $b_\ell = \mathbf{b}\cdot\hat{\mathbf{U}}_0$. For completeness, we added expansion terms to the right-hand side of Eq. (2). These terms, as described in Verdini, A. et al. (2024); Gogoberidze et al. (2013); Hellinger, P. et al. (2013), account for the impact of the solar wind radial expansion on turbulence. In contrast to the terms in this exact relation, these additional terms are second-order structure functions (SFs), written in terms of the velocity and magnetic fields as

$$F_{\mathrm{exp}} \;=\; -\rho_0\frac{V_{\mathrm{sw}}}{2R}\left[\left\langle(\delta\mathbf{u}_\perp)^2\right\rangle \;+\; \left\langle(\delta\mathbf{b}_R)^2\right\rangle\right], \tag{3}$$

where V_{sw} is the solar wind velocity, R is the heliocentric distance, $\mathbf{u}_\perp$ is the component of the velocity perpendicular to the radial direction, and $\mathbf{b}_R$ is the radial component of the Alfvén velocity. These terms quantify the expansion-driven source term in the third-order law and become relevant at large scales, where they can be comparable to the nonlinear transfer estimate, particularly in Alfvénic streams (Verdini, A. et al. 2024).

3. PSP data selection

The magnetic field data were obtained from the fluxgate magnetometer of the FIELDS instrument suite (Bale et al. 2016), while the proton density and velocity data were measured by the Solar Probe Cup (SPC) of the Solar Wind Electrons Alphas and Protons (SWEAP) instrument suite (Kasper et al. 2016; Case et al. 2020). Originally, the magnetic field resolution from FIELDS is 4 Hz on average. These data were interpolated to a 30-second cadence to match the proton density and velocity data. This ensured consistency between the two datasets, which is relevant for computing the energy transfer rate in the next section. We studied 28 time intervals from 01 November 2018 to 22 April 2024, each with a duration of two days. The SPC plasma moments are known to contain spurious spikes, particularly during intervals of low signal or spacecraft maneuvers. To mitigate these effects, we applied a sequence of filters similar to those described in previous works (Brodiano et al. 2023). First, a sharp mean-value filter was used to identify and replace isolated outliers exceeding a fixed threshold relative to adjacent points. Subsequently, a Hampel filter was applied to remove any remaining anomalous values and smooth the resulting time series (Davies & Gather 1993; Liu et al. 2004; Pearson et al. 2016). This procedure effectively eliminated unphysical spikes while preserving the statistical properties of the plasma data, ensuring the reliability of the computed transfer rates.

We only present two representative intervals corresponding to two different heliocentric distances: 0.34 au and 0.44 au. The two-day duration was chosen to access the low-frequency part of the spectrum where $1/f$ is likely to be observed (e.g., Bruno & Carbone 2013). We estimated the correlation time τ_c of the magnetic field data (defined as the time over which the correlation decreases by one e-folding factor ($1/e \approx 0.37$; Wrench et al. 2024; Matthaeus et al. 2005; Cuesta et al. 2022) and performed a convergence test of the correlation length to ensure relative statistical stationarity of the selected samples (Stawarz et al. 2022). The obtained values of τ_c and the derived frequencies f_c are shown in Table 1 for comparison with the spectral break marking the transition from the $1/f$ range to the inertial range. In addition, to ensure the validity of our statistical analysis, we examined the stationarity of the selected two-day intervals. Since such long intervals may not be stationary, we employed the following tests. First, we computed the autocorrelation function (ACF) of the magnetic and velocity fields, where we found that the correlations decay rapidly within the expected confidence bounds, consistent with stationary behavior (see, e.g., Dorseth, Mason et al. 2024). Visual inspection of the time series, together with the evaluation of the mean and the variance in sliding windows, confirmed that these quantities remained approximately constant throughout the intervals (Matthaeus & Goldstein 1982). We also verified the convergence of the spectral slope and mean level in the $1/f$ range, which provides further support for the assumption of statistical stationarity. These results indicate that the first and second moments of the fluctuations can, to some extent, be considered stationary, which legitimizes the use of correlation techniques and temporal averages as estimates of ensemble averages. As an additional selection criterion, we inspected the magnetic field, velocity, and density time series to avoid intervals containing a possible heliospheric current sheet (HCS) crossing. For the second event, for example, gradual variations are observed during the second day, but the selected sample shows no clear magnetic polarity reversal or plasma signature that would allow us to identify an HCS crossing within the analyzed interval. Together with the stationarity and convergence tests described above, this supports the suitability of the selected intervals for the statistical analysis performed here.

4. Observational results and a scale-dependent cascade model

To characterize turbulence in the $1/f$ range, we estimated the energy transfer rate as a function of time lag. Figures 1a and 1c show the nonlinear transfer estimate together with the expansion contribution described above, and the compensated PSD of the magnetic field fluctuations in panels (b) and (d). For all analyzed spectra, distinct ranges exhibiting $1/f$ scaling were observed. In the PSP intervals analyzed here, the expansion term remains systematically smaller than the estimated nonlinear transfer term and does not contribute substantially to the scale-dependent cascade discussed below.

It is important to clarify the interpretation of the third-order law when it is applied to the $1/f$ range. The exact relation used here is derived from the more general von Kármán-Howarth energy balance under the assumptions of statistical stationarity, homogeneity, and negligible dissipation at the scales of interest. A scale-independent cascade rate is therefore not a prerequisite of the formulation itself, but rather a property that characterizes a classical inertial range once verified a posteriori. Since these conditions are not necessarily fulfilled on the largest scales of the solar wind, where the $1/f$ spectrum is typically observed, we did not assume from the outset that this range behaves as a standard inertial range. Instead, we interpreted the third-order estimate in terms of an effective nonlinear transfer rate and examined how it varies with scale. From this perspective, the quantity $\varepsilon(\tau)$ should be interpreted as an effective nonlinear transfer rate and not as a strict Kolmogorov-like dissipation rate. Therefore, the absence of a plateau in $\varepsilon(\tau)$ does not invalidate the third-order estimate; instead, it is precisely the observed scale dependence that carries the physical information about the $1/f$ range. Within this $1/f$ range, the nonlinear transfer rate exhibits a $1/\tau$ scaling (dashed black lines) before nearly flattening at $\tau < \tau_c$, marking the transition to the inertial range. To quantitatively identify the range where the $1/\tau$ scaling of the energy transfer rate holds, we performed a sliding window fit of $\varepsilon(\tau)$. This procedure was applied over consecutive partially overlapping windows of fixed logarithmic width, allowing us to detect the intervals where the local slope remained approximately constant and close to -1. The fact that $\varepsilon(\tau)$ exhibits a systematic scale dependence within the $1/f$ range provides useful information about how nonlinear interactions operate at these large scales and how the classical inertial range assumptions progressively break down as the outer scales of the turbulence are approached.

A tendency for the nonlinear transfer rate to decrease with scale in the $1/f$ range has also been observed in recent studies. In particular, Verdini, A. et al. (2024) reported that the cascade flux is negligible at large scales compared to the effects of expansion. Nevertheless, their results display a clear trend of decay in the $1/f$ range, approximately consistent with a $1/\tau$ dependence. Although not explicitly discussed by the authors, this behavior suggests that nonlinear processes might not be entirely suppressed at the largest scales and that the cascade might instead retain a scale-dependent component, in agreement with our findings. Although we show cases where the sign of the nonlinear energy transfer rate does not change, there are cases in which the transition between the $1/f$ range and the inertial range is characterized by a change in the sign of the cascade rate. The scale-dependent energy transfer rate reflects a non-conservative turbulent cascade and indicates the presence of intermittency (Oboukhov 1962; Frisch 1995).

To provide an explanation for this new scaling law of the nonlinear transfer rate, we turned to classical dimensional analysis. Using Eq. (2) and assuming $\delta\mathbf{u} \sim \delta\mathbf{b} \sim \delta u_\ell \sim \delta b_\ell$, we obtain in the inertial range

$$S_3(\ell) = \langle \delta b_\ell^3 \rangle \sim \varepsilon\, \ell, \tag{4}$$

where ε is assumed constant. We then readily obtain the Kolmogorov spectrum $b_k^2 \sim k^{-5/3}$ from relation (4). Now, we introduce a scale-dependent nonlinear transfer rate ε_ℓ and assume that the Kolmogorov third-order law (4) remains valid in the $1/f$ range. This can be viewed as a tentative extension of the refined self-similarity hypothesis to the $1/f$ range (see discussion below). We then write

$$\delta b_\ell \sim (\varepsilon_\ell\, \ell)^{1/3}. \tag{5}$$

Assuming the cascade rate ε_ℓ obeys a power-law scaling[1], namely $\varepsilon_\ell \sim \ell^\alpha$, and introducing this relation into Eq. (5), we obtain $\delta b_\ell \sim \ell^{(1+\alpha)/3}$. From this relation and following the usual steps of dimensional analysis, we obtain the following scaling of the magnetic energy spectrum:

$$b_k^2 \sim k^{-2(1+\alpha)/3-1}. \tag{6}$$

From relation (6), it is straightforward to infer that if the magnetic energy spectrum scales as $b_k^2 \sim k^{-1}$, then $\alpha = -1$, which in turn yields a scale-dependent nonlinear transfer rate,

$$\varepsilon_\ell \sim \ell^{-1}. \tag{7}$$

This prediction is consistent with the estimated nonlinear transfer rates in Fig. 1 (with $\ell = U_0\,\tau$, where we assumed the Taylor hypothesis). While several models (generally inspired by studies in hydrodynamic turbulence) were used to study intermittency at small scales (i.e., scales belonging to the inertial range),

[1] This assumption allows for obtaining the scaling law (6) directly by integrating Eq. (1).

Table 1. Solar wind plasma parameters for the two events.

Start time [UT]	End time [UT]	$\langle r \rangle$ [au]	U_0 [km/s]	δu_0 [km/s]	U_A [km/s]	M_A	τ_c [s]	f_c [Hz]
2018-11-15 00:00	2018-11-17 00:00	0.34	535.78	44.53	128.40	4.17	326	3.0×10^{-3}
2022-02-12 00:00	2022-02-14 00:00	0.44	411.45	42.04	83.48	4.93	870	1.1×10^{-3}

Notes. From left to right: start and end time of the events in UT, mean value of the heliocentric distance, mean plasma flow speed, root-mean-square value of the outer-scale (energy-containing range) fluid velocity, Alfvén speed, Alfvén Mach number, correlation time, and associated correlation frequency.

our model and observations address intermittency in the $1/f$ range. Moreover, intermittency was tackled through the scale-dependent nonlinear transfer rate, while it is generally analyzed through the field increments (Frisch 1995).

The scale-dependent nonlinear transfer rate $\varepsilon_\ell \sim 1/\ell$ implies a non-conservative cascade: large scales process energy at slower rates than small scales. In the (mathematical) limit $\ell \to +\infty$, $\varepsilon_\ell \to 0$. This behavior is physically consistent with the expectation that nonlinear interactions weaken at the largest scales of the turbulence. In contrast to the inertial range, where the cascade rate is approximately constant due to the conservative nature of the energy transfer, the outer scales are affected by large-scale driving and boundary conditions. As a result, the cascade process is expected to become progressively less efficient as ℓ approaches the integral scale. In this sense, the scale-dependent cascade rate observed in the $1/f$ range might reflect a transitional regime between energy-containing scales and the inertial range.

To provide a physical interpretation of this result, we assumed the existence of an integral scale L_0 in the energy-containing scales as an upper bound on ℓ, with which we associated a large-scale transfer rate $\varepsilon_{L_0} \sim 1/L_0$. At much smaller scales, we assumed that turbulence forms an inertial range whose onset is the correlation scale L_c, where the energy is transferred at a constant rate $\varepsilon_{\mathrm{IR}}$ (i.e., the conservative energy transfer rate in the inertial range). Within these assumptions, the $1/f$ range is bound to process energy at a rate that must fulfill two boundary conditions: $\varepsilon_\ell = \varepsilon_{L_0}$ for $\ell = L_0$, and $\varepsilon_\ell = \varepsilon_{\mathrm{IR}}$ for $\ell = L_c$. These conditions then set the mathematical form (e.g., the slope) of the transfer rate in the energy-containing scales range. Thus, we speculate that the scaling of the transfer rate in this range might not be universal. Instead, the scaling would depend on the system size (namely, the ratio of the integral and correlation lengths L_0/L_c), which fixes the functional form of ε_ℓ to satisfy the boundary conditions at L_0 and L_c. Scalings different from $1/\ell$ will yield different energy spectral slopes. This scenario might explain the variability of magnetic PSD slopes observed in planetary magnetosheaths on the largest scales, where spectral indices other than f^{-1} have frequently been reported (Hadid et al. 2015; Huang et al. 2017).

5. Observational results and intermittency in the $1/f$ range

To characterize intermittency in the $1/f$ range, we estimated the probability density function (PDF) of the magnetic field fluctuations, which we decomposed into parallel and perpendicular components using a sliding-window approach (e.g., Huang et al. 2014). The mean magnetic field within each window defines the parallel direction, while the two perpendicular components are determined through projection. The window width was chosen based on a stationarity criterion using a tolerance of 0.25

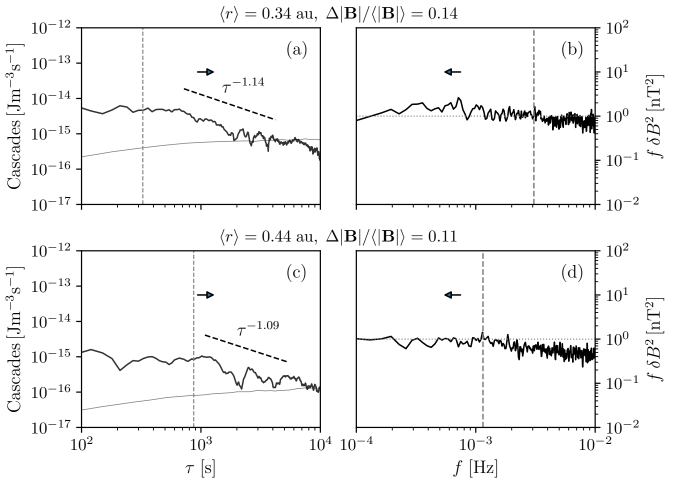

Fig. 1. Panels (a) and (b) correspond to the $\langle r \rangle = 0.34$ au interval, showing the incompressible nonlinear transfer estimate $|\varepsilon|$ (black) with the expansion term $|\mathcal{F}_{\mathrm{exp}}|$ (gray) as a function of the time lag τ, and the compensated PSD, $f\delta B^2$, as a function of the frequency f, respectively. Panels (c) and (d) show the same quantities for $\langle r \rangle = 0.44$ au. The dashed black lines represent power-law fits of the total incompressible nonlinear transfer estimate within the $1/f$ range. The vertical dashed gray lines mark the correlation time τ_c in (a) and (c) and the related correlation frequency f_c in (b) and (d). The horizontal arrows highlight the $1/f$ interval used for the fits in (a) and (c) and the corresponding range in (b) and (d).

to ensure that the local mean field remained representative of the background field throughout the interval. Figure 2 shows the PDFs (normalized to their standard deviation) of the parallel and perpendicular components of the magnetic field increments in the $1/f$ range for the same two samples taken at different heliocentric distances. For comparison, a Gaussian distribution (dashed lines) is overplotted. In all cases, the PDFs of the parallel component deviate significantly from a Gaussian distribution, indicating high levels of intermittency (Matthaeus et al. 2015; Hadid et al. 2015). Our results agree well with the recent findings by Sorriso-Valvo, L. et al. (2023), who analyzed Helios 2 observations in the inner heliosphere. They reported that the $1/f$ range exhibits clear signatures of a turbulent cascade using the third-order law and the emergence of intermittency, particularly in fast solar wind streams. In contrast, the PDFs of the perpendicular increments exhibit a quasi-Gaussian distribution, indicating their random-like nature. This suggests that the parallel fluctuations might have had enough time to evolve nonlinearly, as if they emerged deeper in the corona than the perpendicular fluctuations. The present observations are at odds with the known properties of turbulence in the inertial range of the solar wind, where both parallel and perpendicular fluctuations exhibit highly non-Gaussian statistics (Kiyani et al. 2012). They highlight the

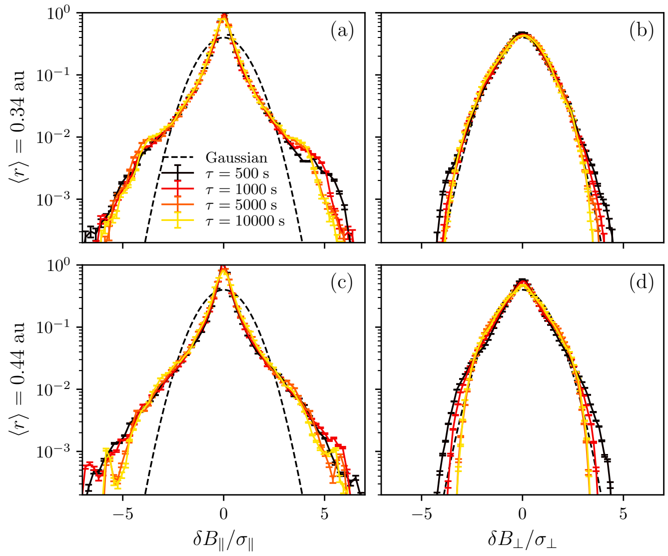

Fig. 2. PDFs of the parallel and perpendicular magnetic field increments for $\tau = \{500, 1000, 5000, 10000\}$ s in the $1/f$ range at heliocentric distances of 0.34 au (panels a and b) and 0.44 au (panels c and d). A Gaussian distribution (dashed black curve) is shown for comparison.

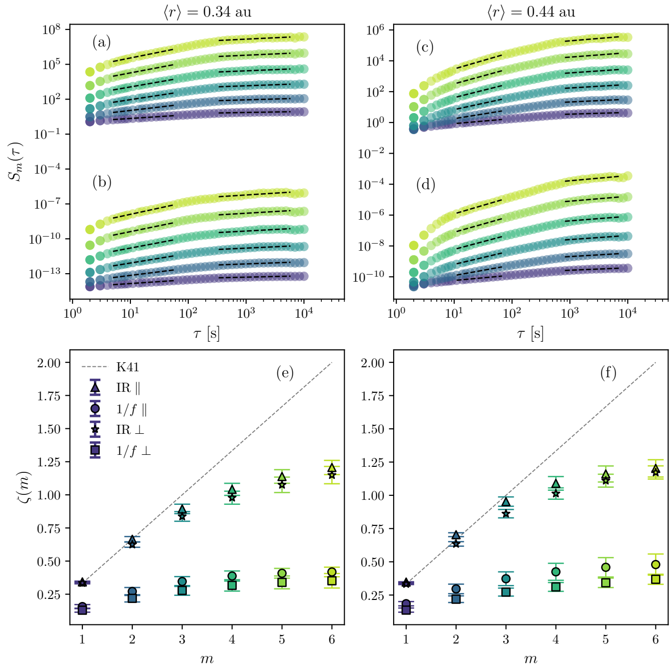

Fig. 3. *Top*: Structure functions of the perpendicular (a and c) and parallel (b and d) fluctuations, $S_m(\tau) = \langle |B_{\perp,\parallel}(t+\tau) - B_{\perp,\parallel}(t)|^m \rangle$, as a function of the time lag τ for different orders m, spanning the $1/f$ and inertial ranges. *Bottom*: Scaling exponent $\zeta(m)$ as a function of the order, obtained from $S_m(\tau) \propto \tau^{\zeta(m)}$, in the inertial range (triangles and stars) and the $1/f$ range (circles and squares). The dashed gray line indicates the prediction from Kolmogorov theory, $\zeta(m) = m/3$, for self-similar turbulent flows.

leading role that appears to be played by the (non-symmetric) heavy tails of the PDF of parallel fluctuations in shaping the scale-dependent transfers in the $1/f$ range. As the cascade proceeds to small scales close to the inertial range, the PDFs of the perpendicular fluctuations become heavy tailed (not shown) and contribute more effectively to the cascade. This explains the increasing transfer rate until the upper bound $\varepsilon_{\rm IR}$ is reached at the scale L_c.

Although the parallel fluctuations are subdominant in amplitude (they only represent ~20-30% of the total fluctuations; (Howes et al. 2014)), they appear to contribute significantly to the transfer signatures observed in the $1/f$ range. This can be understood by noting that the longitudinal increments δu_ℓ and δb_ℓ entering Eq. (2) are quasi-parallel or antiparallel (or moderately oblique) to $\mathbf{B}$, considering average angles $\theta_{vB} = 37°$ and $45°$ for the intervals at 0.34 au and 0.44 au, respectively. Thus, the one-dimensional sampling of the turbulence through the Taylor hypothesis is particularly sensitive to fluctuations with a strong parallel, and therefore compressive, component. Another remark is that the incompressible model we used seems to capture the role of the parallel (compressible) fluctuations. Using the isothermal model of Andrés & Sahraoui (2017) and the polytropic model of Simon & Sahraoui (2021) (not shown here), we found no significant changes in the estimated nonlinear transfer rates to those shown in Fig. 1, remaining quantitatively consistent with the incompressible estimate within the statistical uncertainties. Rather than indicating that compressive effects are negligible, this suggests that the incompressible longitudinal estimate already captures a large fraction of the compressible transfer in these intervals, likely because $\delta b_\ell \sim \delta b_\parallel$ in our sampling geometry. In this sense, the incompressible formulation appears to recover most of the relevant transfer signature even in the presence of compressive fluctuations, which might also indicate that part of the compressive dynamics is controlled by the incompressible one (Schekochihin et al. 2009).

In the inertial range, the self-similarity hypothesis of Kolmogorov theory suggests that for a constant energy transfer rate ε, the structure functions scale dimensionally as

$$S_m(\ell) \sim (\varepsilon\ell)^{m/3}. \tag{8}$$

We used an analogous dimensional argument in the $1/f$ range, but replaced the constant energy transfer rate by the scale-dependent transfer rate ε_ℓ. This gives

$$S_m(\ell) = C_m\,(\varepsilon_\ell \ell)^{m/3}\,, \tag{9}$$

where C_m is an order-dependent coefficient (Frisch 1995). The third-order case has a special status, since third-order structure functions are directly related to the scale-to-scale energy transfer through exact turbulence laws (see, e.g., Andrés et al. 2016, and references therein). However, no analogous exact relation fixes the coefficients C_m for arbitrary orders m. Therefore, Eq. (9) should be regarded as a dimensional self-similar form based on the scale-dependent transfer rate and not as an exact law for all orders.

Since the scaling $\varepsilon_\ell \sim \ell^{-1}$ was inferred from the third-order estimate, the third-order structure function provides a natural constraint for the behavior expected in the $1/f$ range. In particular, if $S_3(\ell) \sim \varepsilon_\ell \ell$ and $\varepsilon_\ell \sim \ell^{-1}$, then $S_3(\ell)$ is expected to be approximately scale independent in this range. A simple self-similar extension of this dimensional argument to higher orders would then suggest that the higher-order structure functions should also display a weak scale dependence, approaching a plateau-like behavior in the $1/f$ range. A more restrictive benchmark is obtained by assuming $C_m = C_3^{m/3}$. This relation can be interpreted as an ansatz for perfect self-similarity. If the increments at each scale were described by a single scale-dependent amplitude, $\delta b_\ell = A(\ell)X$, with $A(\ell) = (\varepsilon_\ell \ell)^{1/3}$ and

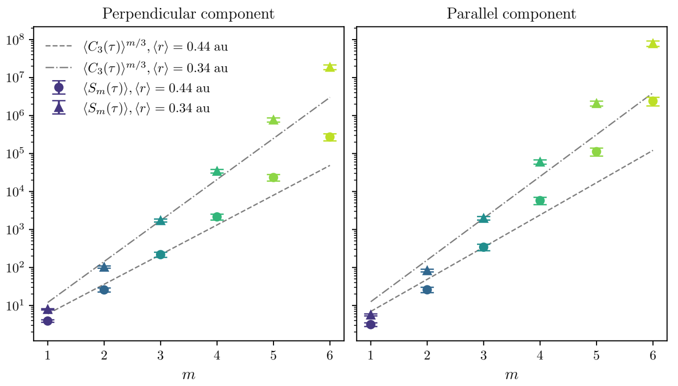

Fig. 4. Estimation of the average coefficient $C_m(\tau)$ in the $1/f$ range (error bars denote one standard deviation) for different orders m of the structure functions (dots), compared with the restrictive self-similar benchmark $C_m = C_3^{m/3}$ (dashed gray line).

a scale-invariant random variable X, then all the scale dependence of the moments would be encoded in $A(\ell)$. The third-order moment as the reference normalization would then lead to $S_m(\ell) \sim [S_3(\ell)]^{m/3}$, and therefore, to the restrictive relation $C_m = C_3^{m/3}$. Departures from this benchmark, together with the non-Gaussian PDFs and the behavior of the scaling exponents $\zeta(m)$, are interpreted as signatures of departures from simple self-similarity in the $1/f$ range. We observe indeed (at the top of Fig. 3) a weak scale-dependence of SFs in the $1/f$ range, in contrast with the scaling in the inertial range. Assuming power-law dependence of the SFs,

$$S_m(\tau) \sim \tau^{\zeta(m)},$$

we can extract the scaling exponents $\zeta(m)$, which are plotted at the bottom of Fig. 3. First, in the inertial range, we recover the known results that turbulence (for parallel and perpendicular fluctuations) is multifractal, as manifested by the clear departure from the Kolmogorov prediction for self-similar flows, $\zeta(m) = m/3$ for $m > 3$. In the $1/f$ range, the dependence of the scaling exponents on m is weaker for parallel and perpendicular fluctuations: the dependence is the weakest for the latter, which likely originates from their quasi-Gaussian statistics shown in Fig. 2. Nevertheless, the dependence of $\zeta(m)$ on m in the $1/f$ range (when statistical error bars are considered) seems to be physical and reflects a scale-dependence of the high-order SFs and the violation of self-similarity. This is further supported by comparing the estimated coefficients C_m with the restrictive self-similar benchmark $C_m = C_3^{m/3}$. The results are shown in Fig. 4. This idealized benchmark slightly departs for increasing-order m, which provides additional evidence of departures from simple self-similarity in the $1/f$ range.

It is expected that the benchmark works reasonably well for the lowest orders. Low-order moments are mostly controlled by typical fluctuations and are therefore less sensitive to rare intermittent events. If the central part of the increment PDFs is approximately self-similar in the $1/f$ range, these moments can remain close to the dimensional prediction based on $(\varepsilon_\ell \ell)^{1/3}$. In contrast, higher-order moments are increasingly sensitive to the tails of the PDFs and to coherent or intermittent structures. Their departure from the benchmark therefore indicates that the scale-dependent cascade is not perfectly self-similar, even though its lower-order statistics can still be organized by the scale-dependent transfer rate.

The intermittent signatures of the $1/f$ range are revealed here through the combined behavior of the scale-dependent mean transfer rate, the higher-order structure functions, and the comparison with the idealized coefficients C_m. An alternative approach would be to consider the local nonlinear transfer rate $\varepsilon_i(\ell)$ as a random variable that reflects different realizations of the flow (here, we only considered its mathematical expectation: $\varepsilon_\ell = \langle \varepsilon_i(\ell)\rangle$). Its intermittent character can be further quantified via its moments, $\varepsilon_\ell^{(m)} = \langle \varepsilon_i^m(\ell)\rangle$.

6. Conclusions

We presented new observations of the $1/f$ range of solar wind turbulence from PSP data. The first result is that the $1/f$ scaling of the magnetic energy spectra in this range reflects a nonconservative cascade at a rate $\varepsilon_\ell \sim 1/\ell$ (assuming the validity of the Taylor hypothesis at these scales). The key point is that the third-order estimate was used here as a diagnostic of nonlinear transfer: when it is not constant, it should not be interpreted as an inertial-range dissipation rate, but as an effective scale-dependent transfer rate. The main caveat is that the notion of scale separation (i.e., locality) used to derive Eq. (2) might not hold on the largest scales involved in the $1/f$ range. For this reason, our results should be read as evidence of scale-dependent nonlinear transfer and not as a claim that the $1/f$ interval is a standard inertial range. The second key result is that the $1/f$ range displays intermittent signatures that are clearest in the parallel fluctuations. At the same time, the comparison with compressible energy transfer rate estimates suggests that the incompressible longitudinal formulation already captures a large fraction of the relevant transfer in our sampling geometry, likely because the measured longitudinal increments are closely related to the parallel magnetic fluctuations. Some evidence of departure from simple self-similarity in the $1/f$ range, based on structure functions of the magnetic field and on the comparison with an idealized self-similar benchmark, was provided. However, a more rigorous model based on the moments of the local scale-dependent transfer rate remains to be developed. Overall, these results call for revisiting the physics of the $1/f$ range in the solar wind and planetary magnetosheaths, and for extending existing turbulence models to scales much larger than those of the inertial range.

Acknowledgements. All authors acknowledge financial support from the ECOS SUD 2022 # A22U02 CNRS / CONICET grant. M.B., F.P., P.D. and N.A. acknowledge financial support from the following grants: PIP Grant No. 11220200101752, UBACyT Grant No. 20020220300122BA and Redes de Alto Impacto REMATE from Argentina. L.H.Z., D.M. and N.A. acknowledge support by the International Space Science Institute (ISSI) in Bern, through ISSI International Team project # 23-591. D.M. is supported by STFC Consolidated Grant ST/X000974/1. The data supporting the findings of this study are openly available in NASA Parker Solar Probe Data Repository (2018).

References

Andrés, N., Mininni, P. D., Dmitruk, P., & Gomez, D. O. 2016, Phys. Rev. E, 93, 063202
Andrés, N. & Sahraoui, F. 2017, Phys. Rev. E, 96, 053205
Andrés, N., Sahraoui, F., Galtier, S., et al. 2018, J. Plasma Phys., 84, 905840404
Andrés, N., Sahraoui, F., Huang, S., Hadid, L., & Galtier, S. 2022, A&A, 661, A116
Bale, S., Goetz, K., Harvey, P., et al. 2016, Space Sci. Rev., 204, 49
Bandyopadhyay, R., Goldstein, M. L., Maruca, B. A., et al. 2020, ApJS, 246, 48
Bemporad, A., Matthaeus, W. H., & Poletto, G. 2008, ApJ, 677, L137
Biskamp, D. 2003, Magnetohydrodynamic turbulence (Cambridge University Press)
Boldyrev, S., Mason, J., & Cattaneo, F. 2009, ApJ, 699, L39

Brodiano, M., Dmitruk, P., & Andrés, N. 2023, Phys. Plasmas, 30, 032903
Bruno, R. & Carbone, V. 2013, Living Rev. Sol. Phys., 10, 2
Case, A. W., Kasper, J. C., Stevens, M. L., et al. 2020, ApJS, 246, 43
Chandran, B. D. G. 2018, J. Plasma Phys., 84, 905840106
Chen, C. H. K., Bale, S. D., Bonnell, J. W., et al. 2020, ApJS, 246, 53
Coburn, J. T., Forman, M. A., Smith, C. W., Vasquez, B. J., & Stawarz, J. E. 2015, Philos. Trans. R. Soc. A: Math. Phys. Eng. Sci., 373, 20140150
Cuesta, M. E., Parashar, T. N., Chhiber, R., & Matthaeus, W. H. 2022, ApJS, 259, 23
Davies, P. & Gather, U. 1993, J. Am. Stat. Assoc., 88, 782
Dmitruk, P. & Matthaeus, W. H. 2007, Phys. Rev. E, 76, 036305
Dorseth, Mason, Perez, Jean C., Bourouaine, Sofiane, Palacios, Juan C., & Raouafi, Nour E. 2024, A&A, 689, A117
Fox, N., Velli, M., Bale, S., et al. 2016, Space Sci. Rev., 204, 7
Frisch, U. 1995, Turbulence: The Legacy of A. N. Kolmogorov (Cambridge University Press)
Gogoberidze, G., Perri, S., & Carbone, V. 2013, ApJ, 769, 111
Hadid, L., Sahraoui, F., & Galtier, S. 2017, ApJ, 838, 9
Hadid, L. Z., Sahraoui, F., Kiyani, K. H., et al. 2015, ApJ, 813, L29
Hellinger, P., Trávníček, P. M., Štverák, S., Matteini, L., & Velli, M. 2013, J. Geophys. Res.: Space Phys., 118, 1351
Howes, G. G., Klein, K. G., & TenBarge, J. M. 2014, ApJ, 789, 106
Huang, S. Y., Hadid, L. Z., Sahraoui, F., Yuan, Z. G., & Deng, X. H. 2017, ApJ, 836, L10
Huang, S. Y., Sahraoui, F., Deng, X. H., et al. 2014, ApJ, 789, L28
Huang, Z., Sioulas, N., Shi, C., et al. 2023, ApJ, 950, L8
Kasper, J. C., Abiad, R., Austin, G., et al. 2016, Space Sci. Rev., 204, 131
Kiyani, K. H., Chapman, S. C., Sahraoui, F., et al. 2012, ApJ, 763, 10
Liu, H., Shah, S., & Jiang, W. 2004, Comput. Chem. Eng., 28, 1635
MacBride, B. T., Forman, M. A., & Smith, C. W. 2005, in ESA Special Publication, Vol. 592, Solar Wind 11/SOHO 16, Connecting Sun and Heliosphere, ed. B. Fleck, T. H. Zurbuchen, & H. Lacoste, 613
MacBride, B. T., Smith, C. W., & Forman, M. A. 2008, ApJ, 679, 1644
Magyar, N. & Doorsselaere, T. V. 2022, ApJ, 938, 98
Manzini, D., Sahraoui, F., Califano, F., & Ferrand, R. 2022, Phys. Rev. E, 106, 035202
Marino, R., Sorriso-Valvo, L., Carbone, V., et al. 2008, ApJ, 677, L71
Masters, A., Achilleos, N., Dougherty, M. K., et al. 2008, J. Geophys. Res.: Space Phys., 113, A10210
Matteini, L., Stansby, D., Horbury, T. S., & Chen, C. H. K. 2018, ApJ, 869, L32
Matthaeus, W. H., Dasso, S., Weygand, J. M., et al. 2005, Phys. Rev. Lett., 95, 231101
Matthaeus, W. H. & Goldstein, M. L. 1982, J. Geophys. Res.: Space Phys., 87, 10347
Matthaeus, W. H. & Goldstein, M. L. 1986, Phys. Rev. Lett., 57, 495
Matthaeus, W. H., Wan, M., Servidio, S., et al. 2015, Philos. Trans. R. Soc. A: Math. Phys. Eng. Sci., 373, 20140154
Matthaeus, W. H., Zank, G. P., Smith, C. W., & Oughton, S. 1999, Phys. Rev. Lett., 82, 3444
Mininni, P. D. & Pouquet, A. 2009, Phys. Rev. E, 80, 025401
NASA Parker Solar Probe Data Repository. 2018, NASA Parker Solar Probe Data Repository, `https://research.ssl.berkeley.edu/data/psp/`, accessed 2025-10-06
Oboukhov, A. M. 1962, J. Fluid Mech., 13, 77–81
Pearson, R., Neuvo, Y., Astola, J., & Gabbouj, M. 2016, EURASIP J. Adv. Signal Process., 2016
Perez, J. C. & Chandran, B. D. G. 2013, ApJ, 776, 124
Politano, H. & Pouquet, A. 1998a, Geophys. Res. Lett., 25, 273
Politano, H. & Pouquet, A. 1998b, Phys. Rev. E, 57, R21
Romanelli, N., Andrés, N., DiBraccio, G. A., et al. 2024, ApJ, 971, 10
Sahraoui, F. 2008, Phys. Rev. E, 78, 026402
Sahraoui, F., Hadid, L., & Huang, S. 2020, Rev. Mod. Plasma Phys., 4
Schekochihin, A. A., Cowley, S. C., Dorland, W., et al. 2009, ApJS, 182, 310
Simakov, A. N. & Chacón, L. 2008, Phys. Rev. Lett., 101, 105003
Simon, P. & Sahraoui, F. 2021, ApJ, 916, 49
Sorriso-Valvo, L., Carbone, V., Noullez, A., et al. 2002, Phys. Plasmas, 9, 89
Sorriso-Valvo, L., Marino, R., Carbone, V., et al. 2007, Phys. Rev. Lett., 99, 115001
Sorriso-Valvo, L., Marino, R., Foldes, R., et al. 2023, A&A, 672, A13
Stawarz, J. E., Eastwood, J. P., Phan, T. D., et al. 2022, Phys. Plasmas, 29, 012302
Stawarz, J. E., Smith, C. W., Vasquez, B. J., Forman, M. A., & MacBride, B. T. 2009, ApJ, 697, 1119
Velli, M., Grappin, R., & Mangeney, A. 1989, Phys. Rev. Lett., 63, 1807
Verdini, A. & Grappin, R. 2015, ApJ, 808, L34
Verdini, A., Grappin, R., Pinto, R., & Velli, M. 2012, ApJ, 750, L33
Verdini, A., Hellinger, Petr, Landi, Simone, et al. 2024, A&A, 690, A265
Verscharen, D., Klein, K. G., & Maruca, B. 2018, in AGU Fall Meeting Abstracts, Vol. 2018, SH53A–07
Wan, M., Servidio, S., Oughton, S., & Matthaeus, W. H. 2010, Phys. Plasmas, 17, 052307
Wrench, D., Parashar, T. N., Oughton, S., de Lange, K., & Frean, M. 2024, ApJ, 961, 182